Engineering Fracture Mechanics 290 (2023) 109454

Contents lists available at ScienceDirect

Engineering Fracture Mechanics

journal homepage: www.elsevier.com/locate/engfracmech

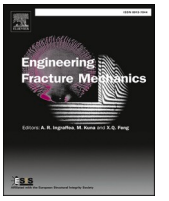

# Mode decoupling in interlaminar fracture toughness tests on bimaterial specimens

Faustino Mujika [a,*], Panayiotis Tsokanas [b,*], Ainhoa Arrese [a], Paolo S. Valvo [c], Lucas F.M. da Silva [d]

[a] Department of Mechanical Engineering, Faculty of Engineering of Gipuzkoa, University of the Basque Country (UPV/EHU), Plaza Europa 1, 20018 San Sebastián, Spain
[b] Institute of Science and Innovation in Mechanical and Industrial Engineering (INEGI), Rua Dr. Roberto Frias, 4200-465 Porto, Portugal
[c] Department of Civil and Industrial Engineering, University of Pisa, Largo Lucio Lazzarino, IT-56122 Pisa, Italy
[d] Departamento de Engenharia Mecânica, Faculdade de Engenharia, Universidade do Porto, Rua Dr. Roberto Frias, 4200-465 Porto, Portugal

ARTICLE INFO

*Keywords:*
Fracture mode decoupling
Bimaterial specimen
Asymmetric double cantilever beam
Asymmetric end-notched flexure
Engesser–Castigliano's theorem

ABSTRACT

The present work has a two-fold objective: (i) to critically review the methods for fracture mode decoupling in unconventional laboratory specimens, such as the asymmetric double cantilever beam (ADCB) specimen; and (ii) to propose mode decoupling conditions and associated specimen design formulae to obtain pure fracture modes when bimaterial specimens are tested in ADCB and asymmetric end-notched flexure (AENF) configurations. In the first part of the paper, the literature on fracture mode decoupling is reviewed to shed light on some controversial points. We start with discussing various pure-mode conditions suggested by different authors and continue with the simplest case of the bimaterial joint. Our review also considers complex cases, such as the presence of bending–extension coupling or residual (hygrothermal) stresses. In the second part of the paper, bimaterial specimens loaded in ADCB and AENF test configurations are investigated. Employing energetically orthogonal mode decomposition, Engesser–Castigliano's theorem, and the laminated beam theory, we illustrate specimen design criteria enabling to obtain pure fracture modes. The obtained specimen design formulae are validated through finite element analyses.

## 1. Introduction

The double cantilever beam (DCB) and end-notched flexure (ENF) tests are the standard procedures for determining the interlaminar fracture toughness of unidirectional laminates in the opening (mode I) and shearing (mode II) fracture modes, respectively. The same tests are commonly used to characterize the interfacial fracture toughness of adhesive bonded joints. Apart from these conventional cases, there is a growing interest in determining the fracture toughness of unconventional specimens, for instance, *asymmetrically* delaminated composites or dissimilar adhesive joints [1]. For this purpose, laboratory coupons are used where the delamination crack is not located on a plane of material and geometric symmetry: e.g., the asymmetric DCB (ADCB) and the asymmetric ENF (AENF) tests (Fig. 1). This asymmetry generally introduces mixed-mode I/II fracture conditions, even if the specimen is subjected to the same loads that produce pure mode I (e.g., Fig. 1a) or pure mode II (e.g., Fig. 1b) conditions in symmetric specimens.

* Corresponding authors.
*E-mail addresses:* faustino.mujika@ehu.eus (F. Mujika), panayiotis.tsokanas@gmail.com (P. Tsokanas).

https://doi.org/10.1016/j.engfracmech.2023.109454
Received 28 April 2023; Received in revised form 21 June 2023; Accepted 28 June 2023
Available online 6 July 2023

**Nomenclature**

| | |
|---|---|
| $a$ | crack length |
| $a$, $a_i$ | extensional compliance |
| $A$, $A_i$ | extensional stiffness |
| $A_i$ | cross-sectional area |
| $b_0$ | length of the cohesive zone |
| $b$, $b_i$ | bending–extension coupling compliance |
| $B$, $B_i$ | bending–extension coupling stiffness |
| $c_1$, $c_{k-1}$, $c_k$ | integration constants |
| $C$ | coenergy |
| $d$, $d_i$ | bending compliance |
| $ds$ | element of arc length along contour $\Gamma$ |
| $D$, $D_i$ | bending stiffness |
| $e$ | sub-beams Young's modulus ratio |
| $E_i$, $E_k$ | longitudinal Young's modulus |
| $F$ | applied force |
| $F^{'}$ | horizontal force reaction |
| $F_C$, $F_T$ | forces in the connection points of the statically determined system |
| $F_j$ | generalized concentrated force |
| $F_n$, $F_t$ | crack-tip normal and tangential forces |
| $G$ | ERR |
| $G_i$ | out-of-plane shear modulus |
| $G_I$, $G_{II}$ | mode I and mode II contributions to the ERR |
| $G_{Ic}$, $G_{IIc}$ | mode I and mode II fracture toughnesses |
| $h$, $h_i$ | thickness |
| $i$ | sub-beam index (unless otherwise stated); $i \in \{1, 2\}$ |
| $I_i$ | moment of inertia |
| $J$ | $J$-integral |
| $J_I$, $J_{II}$ | mode I and mode II contributions to the $J$-integral |
| $k$ | lamina index; $k \in \{1, 2, ..., n\}$ |
| $L$ | half span length of the AENF configuration |
| $M$, $M_i$ | section bending moment |
| $n$ | number of laminae |
| $N$, $N_i$ | section axial force |
| $r$ | sub-beams thickness ratio |
| $s_i$ | shear compliance |
| $S_i$ | shear stiffness |
| $\overrightarrow{T}$ | traction vector |
| $u$ | abscissa indicating horizontal distance |
| $U$, $U^*$ | strain energy and complementary strain energy |
| $V$, $V_i$ | section shear force |
| $w$ | width |
| $W$ | strain energy density |
| $x$ | abscissa indicating horizontal distance |
| $x$, $y$, $z$ | coordinates |
| $X$ | force in the connection point $C$ of the statically determined system |
| $Y$ | contact force |
| $Y_b$, $Y_s$ | bending and shear components of the contact force |
| $z_0, z_1, ..., z_{k-1}, z_k, ..., z_n$ | ordinates of the top and bottom surfaces of laminae |
| $Z$ | force in the connection point $T$ of the statically determined system |
| $\beta_0$ | unbalance parameter |
| $\Gamma$, $\Gamma_I$, $\Gamma_{II}$ | contours surrounding the crack tip |
| $\delta_j$ | generalized displacement |
| $\delta_n$, $\delta_t$ | relative normal and tangential displacements in the cracked region |
| $\overrightarrow{\delta}$ | displacement vector |
| $\Delta$ | displacement of the force-application point |
| $\Delta_n$, $\Delta_t$ | relative normal and tangential displacements at the beginning of the cohesive zone |
| $\varepsilon_0$, $\varepsilon_i$ | axial strain |

| | |
|---|---|
| $\theta$ | rotation angle |
| $\kappa$, $\kappa_i$ | bending curvature |
| $\lambda$ | distance between the two connections of the statically determined system |
| $\nu_{xzi}$, $\nu_{zxi}$ | Poisson's ratios in the $xz$-plane |
| $\sigma$ | interfacial normal stress in the uncracked region |
| $\sigma_x$ | section axial stress |
| $\tau$ | interfacial shear stress in the uncracked region |
| $\tau_{zx}$ | section shear stress |
| ADCB | asymmetric double cantilever beam |
| AENF | asymmetric end-notched flexure |
| DCB | double cantilever beam |
| ENF | end-notched flexure |
| ERR | energy release rate |
| FEA | finite element analysis |
| VCCT | virtual crack closure technique |

To characterize the pure-mode fracture of such asymmetric specimens, several attempts have been made to decouple mode I and mode II through an appropriate specimen design. Ouyang et al. [2], being among the first to focus on this topic, stated that mode decoupling is achieved when the differential equation of the mode I (mode II) fracture is only governed by the interfacial normal (shear) stress and relative normal (tangential) displacement. A similar statement was made by Bennati et al. [3], who provided a more general mode decoupling condition covering the case where both sub-beams of the bimaterial specimen feature a bending–extension coupled behavior. Wang et al. [4] focused on the ADCB configuration and argued that pure mode I fracture is achieved when the axial strains of the two sub-beams along the interface are equal. This assumption led to the same specimen design criterion with Ouyang et al. In contrast, individual authors (e.g., [5]) have appeared in the literature, arguing that mode decoupling is achieved when the bending rigidities of the two sub-beams are equal, without justifying this assumption though.

In the present work, which builds upon a recent work by a subset of the present authors [6], we revisit the mode decoupling problem and again derive the mode decoupling conditions, aiming to resolve the controversial points in the literature regarding the different decoupling conditions. We focus on the ADCB (Fig. 1a) and AENF (Fig. 1b) test configurations, also assuming that both sub-beams are homogeneous and special orthotropic. Our approach is based on Rice's $J$-integral [7]. The work assumes that under pure mode I conditions, the relative tangential displacement at the crack tip is null, while under pure mode II conditions, the resultant of interfacial normal stresses in the uncracked region is null. Using these conditions and by developing a simple mechanical model using Engesser–Castigliano's theorem [8] and laminated beam theory, we derive the mode decoupling conditions for bimaterial specimens loaded using the ADCB and AENF test configurations from scratch. We find that the two conditions to obtain pure mode I in the ADCB test and pure mode II in the AENF test coincide and are aligned with the condition used in part of the existing literature. We also show the results of finite element analyses (FEAs) using the virtual crack closure technique (VCCT) to validate this finding. An excellent agreement was observed between the analytical and numerical results. We hope that the present work helps resolve the confusion in the literature regarding the correctness of different mode decoupling conditions.

The rest of the paper is organized as follows. The state of the art regarding conditions to achieve pure modes and the respective specimen design criteria is presented in Section 2. Next, the mode decoupling conditions adopted in the present work are presented and justified in Section 3. In Section 4, the proposed mode decoupling conditions are employed to determine specimen design criteria for the ADCB and AENF test configurations. Section 5 presents a finite element validation of the proposed specimen design criteria. Lastly, Section 6 summarizes the conclusions of the work.

## 2. Fracture mode decoupling: state of the art

We assume a beam-shaped structure split by a straight crack into two sub-beams. The latter are assumed to have different thicknesses or be made of dissimilar materials (isotropic, orthotropic, or generally layered). Under external loading, the fracture response of such a beam generally is mixed-mode I/II, even if the applied loading corresponds to global opening (mode I) or shearing (mode II).

Several conditions to achieve a pure-mode response have been suggested during the last decades. In addition, some of them have been employed to formulate specimen design criteria mainly for the ADCB test configuration toward pure mode I fracture. These two topics are reviewed below to clarify the confusion still existing in the literature.

### 2.1. Pure-mode conditions

Williams [9] considered an Euler beam made of a homogeneous and isotropic material split by a straight crack into two sub-beams of different thicknesses. Considering that the beam is loaded solely in bending, the author proposed the following two pure-mode conditions for this mixed-mode I/II problem: (i) Pure mode I fracture is obtained if the moments of the two sub-beams at the crack-tip cross section are equal and opposite; (ii) pure mode II fracture is obtained if the curvatures of the two sub-beams at the crack-tip cross section are equal. The reasoning behind choosing these pure-mode conditions was not clarified, but a possible rationale was

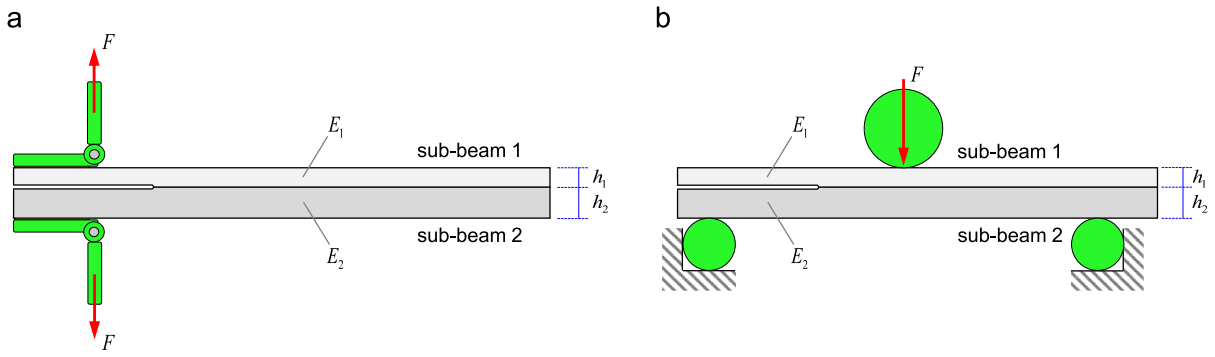


**Fig. 1.** A bimaterial beam specimen loaded using the (a) ADCB and (b) AENF test configurations.

given in Ref. [10]: (i) Since mode I is produced by normal displacement solely, mode II can be ensured by zeroing the relative normal displacement between the two crack surfaces at the crack tip; (ii) since mode II is created by tangential displacement only, mode I is ensured if the relative tangential displacement between the two crack surfaces is set equal to zero. If, however, this rationale is correct, the condition for pure mode I is not generally fulfilled in the case that the two sub-beams have different thicknesses [11].

Although Williams's pure-mode conditions have been questioned in the literature, they have since been used by several authors. For example, Shahverdi et al. [12,13] extended these conditions for the case where the beam is the assemblage of two dissimilar sub-beams made of orthotropic materials. Next, the authors followed both Williams's pure-mode conditions, assuming, however, that the curvatures of both sub-beams depend on their bending stiffnesses (not on the thickness). More recently, Arouche et al. [14] also dealt with the bimaterial case and altered Williams's condition for pure mode I. The authors relied on a strain-based design criterion for ADCB tests on bimaterial joints [4]. This criterion suggests that pure mode I is ensured if the axial strains of the two sub-beams are equal along the interface. To ensure this equality, Williams's condition for pure mode I was modified by introducing a parameter that is a function of Young's moduli and thicknesses of the two sub-beams—more information is given in Section 2.2.

An alternative set of pure-mode conditions has been proposed by Valvo [15–17]. Valvo [15] demonstrated that the (standard) VCCT may be inappropriate to analyze problems involving highly asymmetric cracks since negative values for either mode I or mode II contribution to the energy release rate (ERR) may be calculated, which is physically unacceptable in the author's opinion. This limitation was found to originate from the lack of energetic orthogonality between the two Cartesian components of the crack-tip force used to compute the two modal contributions to the ERR. To remedy this shortcoming, the author suggested the following pure-mode conditions: (i) Pure mode I fracture is obtained if the crack-tip tangential force is zero; (ii) pure mode II fracture is obtained if the crack-tip normal displacement is zero. In a subsequent paper, however, Valvo [16] called into question these conditions and proposed the following ones in their place: (i) Pure mode I fracture is obtained if the crack-tip tangential displacement is zero; (ii) pure mode II fracture is obtained if the crack-tip normal force is zero. In both proposals, the two pure modes are associated to energetically orthogonal systems of forces, so always non-negative mode I and II contributions to the ERR are obtained. This "revised" VCCT formulation was later extended by introducing suitable contact constraints to prevent local interpenetration of the crack-tip nodes [17].

Wang, Harvey and co-workers, in a series of papers, thoroughly studied the problem of mode partitioning of interfacial cracks between both isotropic and laminated beams [18–21]. Among other contributions, they proposed an energy-orthogonal pure-mode methodology toward partitioning the ERR into its mode I and mode II components. In short, the mode I loading condition must be orthogonal to the mode II loading condition through ERR "space". This finding enables us to identify any pure-mode condition by any means—experimentally, for example using digital image correlation measurement to determine the load condition that produces zero relative tangential displacement just behind the crack tip, or by theoretical modeling, or by numerical simulation—, and then use the orthogonality condition to determine all the other pure modes. The authors also defined two sets of locally pure modes:

- Set 1: (i) Pure mode I fracture is obtained if the crack-tip relative tangential displacement is zero; (ii) pure mode II fracture is obtained if the crack-tip normal force is zero.
- Set 2: (i) Pure mode I fracture is obtained if the crack-tip tangential force is zero; (ii) pure mode II fracture is obtained if the crack-tip relative normal displacement is zero.

Interestingly, their first and second sets of pure modes correspond to the two alternative pure-mode conditions suggested by Valvo in Refs. [16] and [15], respectively.

Valvo [22] proposed an analytical method that aimed to "retrieve the spirit of Williams" [p. 117] and determine the ERR and mode mixity based solely on beam theory. Thus, Valvo's method may be seen as an extension of Williams's method to a generally layered beam, potentially with a bending–extension coupled behavior, which features an asymmetric crack. The author considered all the three crack-tip internal forces as he modeled the crack tip using a rigid joint model. Using the definition of the crack-tip displacement rates, Valvo computed the ERR and its mode I and mode II components via an adaption of his "revised" VCCT introduced above. In particular, the following two pure-mode conditions were employed: (i) Pure mode I fracture is obtained if the relative tangential

displacement at the crack tip is zero; (ii) the crack-tip forces and moment should be partitioned into the sum of two energetically orthogonal systems. The first condition coincides with the first condition described by Wang, Harvey, and co-workers [18–21], while the second one ensures that no *coupling* ERR term arises.

### 2.2. Specimen design criteria

We now return to the case of the ADCB test configuration, shown in Fig. 1a, which has emerged as a modification of the standard DCB test also to enable us investigate the interfacial fracture between dissimilar materials, such as adhesive joints between metals and composites. As shown in Fig. 1a, the ADCB specimen can consider both material and geometric *asymmetry* with respect to the delamination plane, as it consists of two sub-beams of different longitudinal Young's moduli, $E_i$, and thicknesses, $h_i$, where $i \in \{1, 2\}$.

Therefore, a reasonable question that has occupied the literature for a long time is whether we can appropriately design the specimen (e.g., define longitudinal Young's moduli and thicknesses of both sub-beams) to achieve pure-mode I conditions. If this was impossible, the ADCB test can only provide us with the total ERR, so an accurate *mode partitioning* approach [23] is necessary to deduce the pure-mode fracture toughnesses of the specimen at hand.

Two mode decoupling conditions can be recognized in the literature:

- Mode decoupling condition (1): Mode decoupling is achieved when the differential equation of the mode I fracture is only governed by the interfacial normal stress and relative normal displacement [2,4,24,25]
- Mode decoupling condition (2): Mode decoupling is achieved when the bending rigidities of the two sub-beams are equal [5,26–29]

Those two conditions are presented below.

#### 2.2.1. Mode decoupling condition (1): decoupled differential equation

Ouyang et al. [2,24] were the first to study this problem. Focusing on the case of a bimaterial beam loaded in mode I, they stated that mode decoupling is achieved when the differential equation of the mode I (mode II) fracture is only governed by the interfacial normal (shear) stress and relative normal (tangential) displacement. Based on this condition and employing an elastic-interface model, they reached the following mode decoupling condition:

$$\frac{h_1}{D_1} = \frac{h_2}{D_2} \tag{1}$$

where $D_i$ is the bending stiffness of sub-beam $i$. Eq. (1) can be reduced to the following one if the Poisson's ratios of the two sub-beams are equal (or very close):

$$E_1 h_1^2 = E_2 h_2^2 \tag{2}$$

In an independent work, Wang et al. [4] suggested that pure mode I is achieved if the two sub-beams have equal axial strains along the interface. As the authors stated, this condition was introduced to remove the relative tangential displacement that is associated to the mode II component. After simple calculations, the authors also obtained Eq. (2).

#### 2.2.2. Mode decoupling condition (2): equal bending rigidities

Another mode decoupling condition for bimaterial ADCB specimens was first proposed by Boeman et al. [5]. The authors stated that the two sub-beams should have equal bending stiffnesses to achieve a pure mode I fracture:

$$E_1 I_1 = E_2 I_2 \tag{3}$$

where $I_i$ denotes the moment of inertia. The design formulae can also be expressed as

$$E_1 h_1^3 = E_2 h_2^3 \tag{4}$$

Although requiring equal bending stiffnesses sounds reasonable, it is just an assumption that has not emerged from a mechanical model. Nevertheless, Eq. (4) has since been adopted in several works that aim to design bimaterial specimens toward pure mode I [5,26–29], usually without justification of this selection though.

### 2.3. Comparison based on evidence in the literature

Inspecting Eqs. (1) and (4), we observe that the two design formulae differ in the power to which the thicknesses are raised: square power versus cubic power. Of course, the interest is in which of the two conditions is right.

The authors who follow the first criterion [2,4,24,25] clearly indicate its suitability. The experimental work by Ouyang et al. [2] shows that the relative tangential displacement near the crack tip is significantly suppressed. In addition, fractographic evidence by Wang et al. [4] demonstrates the absence of features on the fracture surface related to the mixed-mode process, an indication of the absence of mode II fracture. Moreover, the FEA results reported by Zambelis et al. [25] show that the mode II contribution to the ERR is zero in their bimaterial DCB joints designed following the first criterion.

The authors who use the second criterion [5,26–29] claim that the shear loading of the DCB specimen can be minimized by using

the condition given by Eq. (4). In contrast, in some of the numerical results presented [26], there is a small contribution of mode II. This may be a good indication of the design approach of matching the bending stiffnesses of both sub-beams fails to guarantee a purely mode I condition. Nevertheless, the accuracy achieved by design criterion 2 is sometimes satisfactory for practical applications, which does not make its use prohibiting.

### 2.4. More complex cases

Although the ADCB specimen is the one predominantly used in the literature, the AENF specimen is also an option to study the interfacial fracture of bimaterial configurations. Ouyang and Li [30] were the first to study the mode decoupling of this specimen, and, using the same modeling with Ref. [2], they obtained the same specimen design formula (i.e., Eqs. (1) and (2)). Moreover, we should not overlook that both Eqs. (1) and (2) are particular cases, for sub-beams made of homogeneous and special orthotropic materials, of the balance condition $\beta_0 = 0$ that has been stated by Liu et al. [31] and Bennati et al. [3], and by Tsokanas and Loutas [32] in a different notation.

The above brief review shows that designing ADCB test specimens toward pure-mode conditions is well established for bimaterial joint cases, although a disagreement clearly exists in the literature. In more complex cases, such as when any of the sub-beams is bending–extension coupled, no specimen design formulae are available to the best of our knowledge. To manage this problem, Garulli et al. [33,34] proposed designs of fully uncoupled laminates that cancel out the effect of an elastically coupled behavior. Moreover, the presence of residual (hygro)thermal stresses on the joint, which is likely to happen for a bimaterial joint, complicates the finding of a mode decoupling solution. More specifically, the existing literature on this topic (e.g., [35,36]) strongly indicates that pure-mode conditions cannot be maintained throughout the ADCB test of a dissimilar specimen with residual (hygro)thermal stresses.

The work by Davidson et al. [37] should also be mentioned, where an alternative, approximate solution for mode decoupling is proposed. Additionally, Jespersen et al. [38] proposed a testing approach to experimentally cancel out the thermal stresses in bimaterial joints.

Therefore, in the presence of bending–extension coupling or residual hygrothermal stresses, the existing literature, which basically concerns the ADCB test configuration and thus lacks generality, cannot provide accurate design solutions to achieve mode decoupling. In such cases, the need for a successful mode partitioning approach is highlighted to extract the values of the pure-mode contributions to the ERR of a given material system from a mixed-mode test. Based on the above points, recent work [32,36] was moved away from the logic of mode decoupling and is focused on mode partitioning [23], which has general applicability.

## 3. The proposed mode decoupling conditions

After reviewing the state of the art, we here present the mode decoupling conditions employed in the present study. Our selection was based on this state of the art, as explained below.

### 3.1. J-integral formulation

Rice [7] defined the path independent $J$-integral calculated on a closed curve that includes the crack tip. In the case of a linearly elastic material behavior, the $J$-integral coincides with the ERR, $G$ [39,40]. The decoupling conditions can be based on the $J$-integral determined when the curve is the contour of the cohesive zone (see Fig. 2a), and the relevant derivation is provided in Ref. [41].

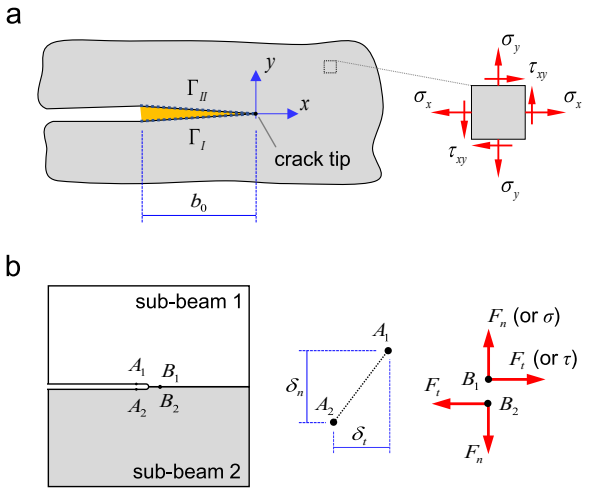


**Fig. 2.** (a) Cohesive zone of length $b_0$, the path, $\Gamma$, used to determine the $J$-integral, and notation for the in-plane stresses; (b) notation for the relative displacements in the cracked region and crack-tip forces or stresses.

The $J$-integral is defined as

$$J = \int_{\Gamma} W dy - \vec{T} \cdot \vec{\delta}_{,x} ds \tag{5}$$

where $\Gamma$ is an arbitrary contour surrounding the crack tip; $W$ is the strain energy density; $\vec{T}$ is the traction vector, defined according to the outward normal, $\hat{n}$, along $\Gamma$; $\vec{\delta}$ is the displacement vector; $ds$ is an element of arc length along $\Gamma$; and comma indicates differentiation. The $J$-integral is evaluated in a counterclockwise sense, starting from the lower surface of the cohesive zone, and continuing along path $\Gamma$ to the upper surface.

Here, $\Gamma$ is chosen to be coincident with the crack surfaces in the cohesive zone, as shown in Fig. 2a. Considering that $dy = 0$, Eq. (5) becomes

$$J = -\int_{\Gamma} \vec{T} \cdot \vec{\delta}_{,x} ds \tag{6}$$

According to the reference system and notation for the in-plane stresses in Fig. 2a,

$$\hat{n} = n_x \hat{i} + n_y \hat{j}, \qquad \vec{T} = \left(\sigma_x n_x + \tau_{xy} n_y\right)\hat{i} + \left(\tau_{xy} n_x + \sigma_y n_y\right)\hat{j}, \qquad \text{and} \qquad \vec{\delta} = u\hat{i} + v\hat{j} \tag{7}$$

The contour $\Gamma$ is divided into $\Gamma_I$ and $\Gamma_{II}$, corresponding to the lower and upper surfaces of the cohesive zone, respectively. The normal vectors and elements of arc length of $\Gamma_I$ and $\Gamma_{II}$ are $\hat{n}_I = -\hat{j}$, $ds_I = dx$ and $\hat{n}_{II} = \hat{j}$, $ds_{II} = -dx$, respectively. Considering Eq. (7), Eq. (6) becomes

$$\begin{aligned} J &= -\left[\int_{\Gamma_I} \vec{T}_I \cdot \vec{\delta}_{I,x} ds_I + \int_{\Gamma_{II}} \vec{T}_{II} \cdot \vec{\delta}_{II,x} ds_{II}\right] = \\ &= -\left[\int_{-b}^{0} \left(-\tau_{xy} u_{I,x} - \sigma_y v_{I,x}\right) dx + \int_{0}^{-b} \left(\tau_{xy} u_{II,x} + \sigma_y v_{II,x}\right)(-dx)\right] = \\ &= \int_{0}^{-b} \sigma_y \delta_{n,x} dx + \int_{0}^{-b} \tau_{xy} \delta_{t,x} dx \end{aligned} \tag{8}$$

In Eq. (8), the relative normal displacement and relative tangential displacement, also shown in Fig. 2b, are respectively defined as

$$\delta_n(x) = v_{II}(x, 0^+) - v_I(x, 0^-) \qquad \text{and} \qquad \delta_t(x) = u_{II}(x, 0^+) - u_I(x, 0^-) \tag{9}$$

Given that the relative displacements of the cohesive zone are functions of $x$, we have

$$d\delta_n(x) = \delta_{n,x} dx \qquad \text{and} \qquad d\delta_t(x) = \delta_{t,x} dx \tag{10}$$

Furthermore, the integral limits in Eq. (8) change as follows:

$$\begin{cases} \text{For } x = -b: \ \delta_n = \Delta_n, \ \delta_t = \Delta_t \\ \text{For } x = 0: \ \delta_n = 0, \ \delta_t = 0 \end{cases} \tag{11}$$

where $\Delta_n$ and $\Delta_t$ are the values at the crack tip (or at the beginning of the cohesive zone). Being $\sigma = \sigma_y$ and $\tau = \tau_{xy}$, and substituting Eqs. (10) and (11) into (8), we get

$$J = \int_{0}^{\Delta_n} \sigma[\delta_n(x), \delta_t(x)] d\delta_n(x) + \int_{0}^{\Delta_t} \tau[\delta_n(x), \delta_t(x)] d\delta_t(x) \tag{12}$$

The derivation of Eq. (12) does not depend on the length of the cohesive zone, $b_0$, and is valid for brittle fractures, where the cohesive zone is small.

### 3.2. The proposed mode decoupling conditions

The first and second integrals in Eq. (12) are the mode I and mode II contributions to $J$, respectively. Consequently, if the second integral is null, pure mode I conditions prevail ($J = J_I$); if the first integral is null, pure mode II conditions prevail ($J = J_{II}$).

The following mode decoupling conditions are employed in the present work:

- Pure mode I fracture is obtained if the relative tangential displacements are zero in the cracked region:

$$\delta_t = 0 \tag{13}$$

- Pure mode II fracture is obtained if the interfacial normal stresses are zero in the uncracked region:

$$\sigma = 0 \tag{14}$$

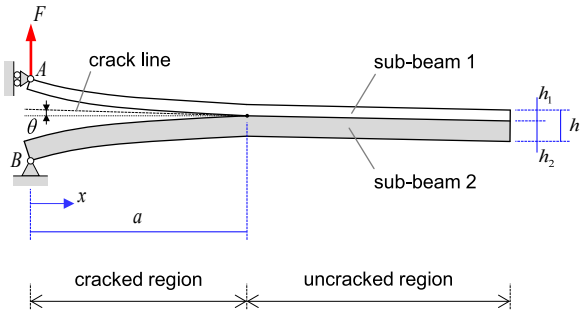


**Fig. 3.** ADCB test configuration.

These conditions have also been reported in the literature. As detailed in Section 2.1, Valvo's [15–17] "revised" VCCT reaches mode decoupling conditions similar to those in Eqs. (13) and (14) for pure modes I and II, respectively. Moreover, similar decoupling conditions have been employed by Wang, Harvey, and co-workers [18–21].

## 4. Specimen design criteria for the ADCB and AENF configurations

The above mode decoupling conditions are now employed to derive specimen design criteria for the ADCB and AENF test configurations. Our analysis is based on Engesser–Castigliano's theorem, unit-load method, and laminated beam theory.

### 4.1. ADCB test configuration

We consider the ADCB configuration shown in Fig. 3. The specimen consists of two sub-beams $i$, $i \in \{1, 2\}$, with dissimilar material properties and thicknesses, perfectly connected along the uncracked region and entirely separated along the cracked region. The specimen has a total thickness of $h$, width (not shown in the figure) of $w$, and (initial) crack length of $a$, while $h_i$ are the thicknesses of the two sub-beams. Both sub-beams can generally be made of a layered material. The specimen is simply supported at point $A$ and pinned at point $B$, while it is loaded in opening through applying a vertical force of intensity $F$ at point $A$.

The dissimilarity of the two sub-beams in terms of material properties and thicknesses introduces an asymmetry with respect to the delamination plane. Thus, the initially horizontal crack line starts to rotate upon loading by a rotation angle θ, as shown in Fig. 3. In other words, shear (or mode II) loading is introduced to the crack tip. We, however, aim to obtain a pure mode I fracture at the crack tip, so we will impose the mode decoupling condition given by Eq. (13).

#### 4.1.1. Engesser–Castigliano's theorem

Engesser–Castigliano's theorem [8], outlined in Appendix A, is used to determine the relative tangential displacement in the crack region, $\delta_t$. We first define an equivalent statically determined system to the ADCB configuration. This system can consist of the two connections at points $T$ (coincident with the crack tip) and $C$—indicating *tension* and *compression*, respectively—that are shown in Fig. 4. The connection at point $T$ prevents the relative normal and tangential displacements, and the connection at point $C$ prevents the relative normal displacement. The distance, $\lambda$, between the two points is generally unknown.

The stress state in the uncracked region of the specimen is unknown. Thus, only the cracked region is considered as a first approach. The rotation angle, θ, shown in Fig. 3, is

$$\theta = d_1 \int_0^a M_1 M_1^{'} dx + d_2 \int_0^a M_2 M_2^{'} dx \tag{15}$$

where $d_i$ is the bending compliance, $M_i$ is the bending moment, and $M_i^{'}$ is the derivative of $M_i$. If the sub-beam is made of a homo-

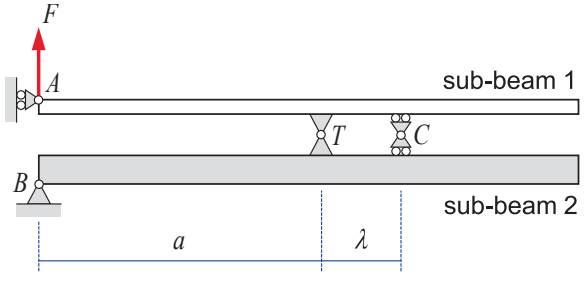


**Fig. 4.** Statically determined system to the ADCB test configuration.

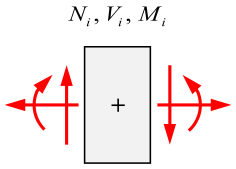


**Fig. 5.** Sign convention for section forces and moment.

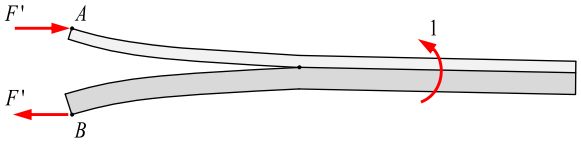


**Fig. 6.** Application of a unitary bending moment.

geneous and special orthotropic material, $d_i = (E_i I_i)^{-1}$, where $E_i$ is the longitudinal Young's modulus and $I_i$ the moment of inertia.

The sign convention used for the section force measures is shown in Fig. 5. This sign convention will be used throughout the paper.

#### 4.1.2. Unit-load method

The unit-load method is now employed to determine $M_i^{'}$. A unitary bending moment is applied in a section of the uncracked region of the specimen, as shown in Fig. 6. As a result, horizontal force reactions, $F^{'} = \frac{1}{h}$, are created at points $A$ and $B$. In the cracked region of the specimen ($0 < x < a$), the bending moments and their derivatives are given as follows:

$$M_1 = Fx, \qquad M_1^{'} = \frac{h_1}{2h}, \qquad M_2 = -Fx, \qquad \text{and} \qquad M_2^{'} = \frac{h_2}{2h} \tag{16}$$

Substituting Eqs. (16) into (15), we get

$$\theta = \frac{Fa^2}{4h}(h_1 d_1 - h_2 d_2) \tag{17}$$

We now assume a rigid-body rotation of the configuration in Fig. 3, so that the crack line becomes horizontal and a relative tangential displacement between points $A$ and $B$ has consequently been introduced. The rotated configuration is shown in Fig. 7. As shown in this figure, the support system has changed: the specimen is now clamped at its right end. The force and moment reactions are null at the clamped end because the pair of applied forces, $F$, satisfies equilibrium. Nevertheless, this clamping condition is necessary to prevent rigid-body motion. The relative tangential displacement between points $A$ and $B$, shown in Fig. 7, is

$$\delta_i^{A,B} = \theta h = \frac{Fa^2}{4}(h_1 d_1 - h_2 d_2) \tag{18}$$

Likewise, the relative tangential displacement between two homologous points along the cracked region can be determined using the unitary forces shown in Fig. 8a. Fig. 8b shows the unitary forces applied at the basic statically determined system of Fig. 4, after having determined reactions. It is inferred that the derivatives of section forces and moments are null between $T$ and $C$. Consequently, the integrals in Engesser–Castigliano's theorem are null as well; see Eq. (15). Hence, the stress distribution in the uncracked region, whatever it is, does not affect the determination of the relative tangential displacement. For every $u < x < a$, the derivatives of the section forces and moments associated to non-zero integrals are

$$M_1^{'} = -\frac{h_1}{2} \qquad \text{and} \qquad M_2^{'} = -\frac{h_2}{2} \tag{19}$$

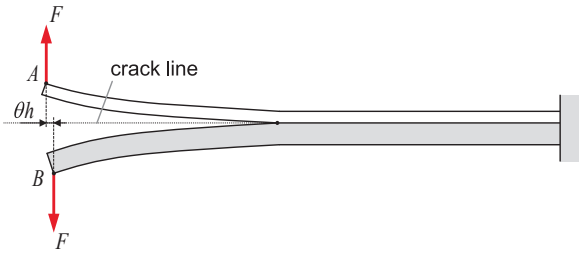


**Fig. 7.** Rotated ADCB configuration with a horizontal crack line.

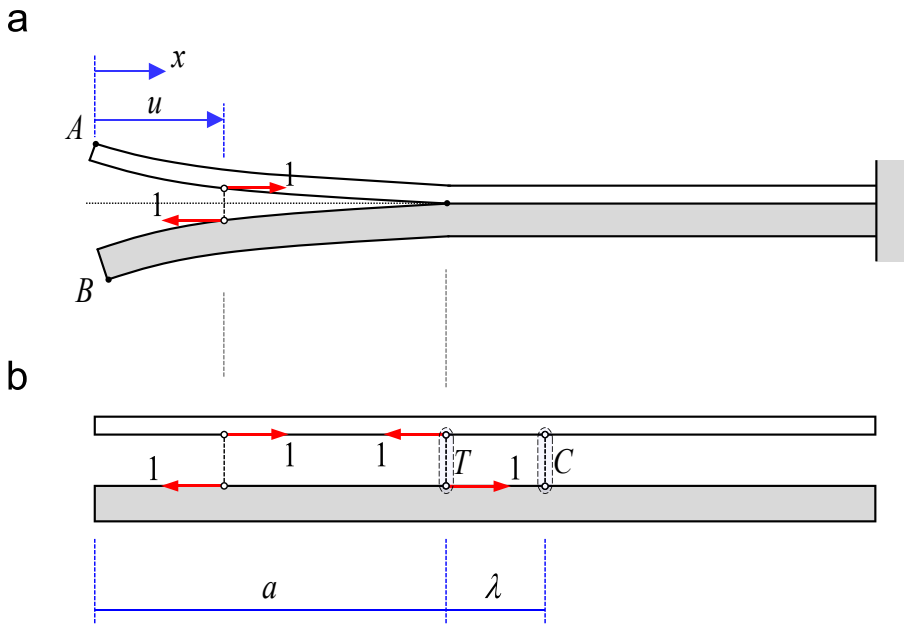


**Fig. 8.** Unitary forces applied to determine the relative tangential displacement, $\delta_t$, between two homologous points: (a) actual system and (b) equivalent statically determined system.

In this case, the relative tangential displacement is

$$\delta_t = d_1 \int_u^a M_1 M_1^{'} dx + d_2 \int_u^a M_2 M_2^{'} dx \tag{20}$$

Substituting the expressions for the moments of Eq. (16) and those for the moment derivatives of Eq. (19) into Eq. (20), we get

$$\delta_t(u) = \frac{F}{4}\left(a^2 - u^2\right)(h_2 d_2 - h_1 d_1) \tag{21}$$

For $u = 0$, Eq. (21) obviously agrees with Eq. (18).

#### 4.1.3. *Specimen design criterion*

For any $u$ value, $\delta_t$ is null if

$$h_1 d_1 - h_2 d_2 = 0 \tag{22}$$

This condition has also been reported in Ref. [2]. If the two sub-beams are made of homogeneous and special orthotropic materials, $d_i = (E_i I_i)^{-1}$, where $E_i$ is the longitudinal Young's modulus. Thus, Eq. (22) becomes

$$\frac{h_2}{h_1} = \sqrt{\frac{E_1}{E_2}} \tag{23}$$

This simple specimen design criterion agrees with part of the existing literature [2,4], as discussed in Section 2.

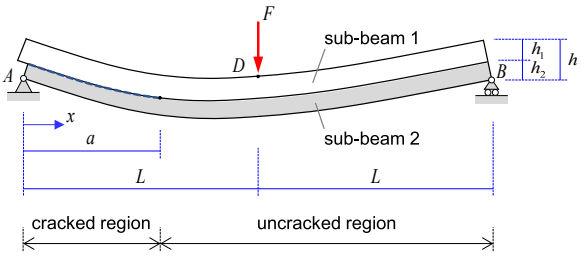


**Fig. 9.** AENF test configuration.

### 4.2. AENF test configuration

Fig. 9 shows the AENF configuration under consideration. Similarly to the ADCB specimen, the AENF specimen is assumed to consist of two sub-beams $i$, $i \in \{1, 2\}$, with dissimilar material properties and thicknesses, which are perfectly connected along the uncracked region and entirely separated along the cracked region. The specimen has a total thickness of $h$, width (not shown in the figure) of $w$, (initial) crack length of $a$, and span length of $2L$, while $h_i$ are the thicknesses of the two sub-beams. Each sub-beam can generally be made of a layered material. The specimen is pinned at point $A$ and simply supported at point $B$, while it is loaded in shearing (or mode II) through a vertical, downwards force of intensity $F$ at point $D$.

The material and geometric asymmetry of the specimen with respect to the delamination plane introduces some opening (or mode I) contribution at the crack tip. Nevertheless, we aim to obtain pure mode II conditions at the crack tip, so we will impose the mode decoupling condition given by Eq. (14).

#### 4.2.1. Contact condition and internal forces

Fig. 10 focuses on the cracked end of the AENF configuration. We assume that contact between the two cracked arms occurs only above the left support (see Fig. 10a). Thus, it is assumed that the load transfer between the two sub-beams is concentrated at one point, and both cracked arms are subjected to a vertical contact force, $Y$, as shown in Fig. 10b.

Fig. 11 shows a free-body diagram of the two sub-beams. The unknown stress distribution in the uncracked region has been reduced to a system of concentrated normal and shear forces, $F_T$, $F_C$, $X$, and $Z$, which are unknown. A pair of contact forces, $Y$, is applied in the left cross section of the specimen, while the section forces and moments at an arbitrary cross section of the uncracked region are also shown.

#### 4.2.2. Engesser–Castigliano's theorem and contact force

We assume that the contact force, $Y$, depends only on the coenergy of the cracked region. Considering bending and shear effects, $Y$ can be determined through Engesser–Castigliano's theorem (see Appendix A) in the following form:

$$C_{,Y} = 0 \Rightarrow d_1 \int_0^a M_1 M_{1,Y} dx + s_1 \int_0^a V_1 V_{1,Y} dx + d_2 \int_0^a M_2 M_{2,Y} dx + s_2 \int_0^a V_2 V_{2,Y} dx = 0 \tag{24}$$

where $M_{i,Y}$ and $V_{i,Y}$ respectively are the derivatives of the section bending moments and section shear forces with respect to $Y$, and $s_i$ is the shear compliance. If the sub-beam is made of a homogeneous and special orthotropic material, $s_i = \frac{6}{5}(G_i A_i)^{-1}$, where $G_i$ is the out-of-plane shear modulus, and $A_i$ is the cross-sectional area.

The section forces and moments and their derivatives are given as follows:

$$\begin{aligned} &V_1 = Y, \quad V_{1,Y} = 1, \quad V_2 = \frac{F}{2} - Y, \quad V_{2,Y} = -1; \\ &M_1 = Yx, \quad M_{1,Y} = x, \quad M_2 = \left(\frac{F}{2} - Y\right)x, \quad M_{2,Y} = -x \end{aligned} \tag{25}$$

Substituting Eq. (25) into (24) and performing some analytical calculations, the contact force takes the form

$$Y = \frac{F}{2} \frac{d_2 a^2 + 3 s_2}{a^2 (d_1 + d_2) + 3(s_1 + s_2)} \tag{26}$$

This force can be decomposed into two components related to bending and shear contributions, respectively:

$$Y = Y_b + Y_s \tag{27}$$

where

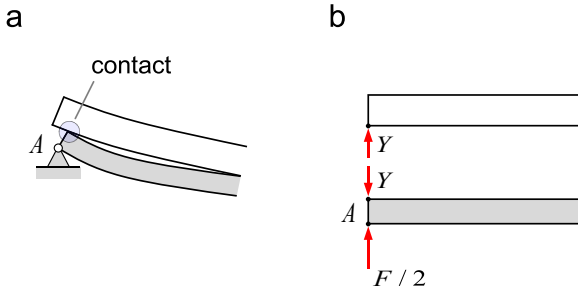


**Fig. 10.** (a) Contact condition in the cracked end of the AENF configuration and (b) contact force, $Y$.

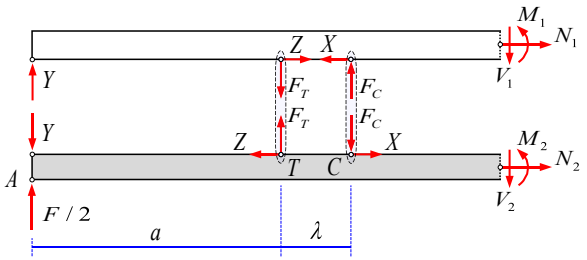


**Fig. 11.** Force diagram for the AENF configuration.

$$Y_b = \frac{F}{2}\frac{d_2}{d_1+d_2} \quad \text{and} \quad Y_s = \frac{F}{2}\frac{s_2 d_1 - s_1 d_2}{(d_1+d_2)[a^2(d_1+d_2)+3(s_1+s_2)]} \tag{28}$$

The bending component in Eq. (28) is obtained considering only bending effects in Eq. (26). Then, the shear component is obtained as $Y_s = Y - Y_b$. As, however, $Y_s << Y_b$, the shear component will be considered negligible below, so $Y = Y_b$.

#### 4.2.3. Equilibrium conditions toward pure mode II

According to Eq. (14), the interfacial normal stresses in the uncracked region, $\sigma$, should be null to achieve pure mode II conditions. As shown in Fig. 11, these normal stresses have been reduced to a system of resultant forces of tensile stresses, $F_T$, and those of compressive stresses, $F_C$. Then, the system constituted by both forces $F_T$ and $F_C$ must have null resultant force and null resultant moment at any point (e.g., at point $C$). This condition is fulfilled if $F_T = F_C = 0$.

Then, to obtain pure mode II, we also impose equilibrium of vertical forces in the upper sub-beam, as follows (see Fig. 11):

$$V_1 = Y_b \tag{29}$$

where $V_1$ is the section shear force of the upper sub-beam along the uncracked region.

The section forces and moments are non-zero to the right of point $C$ (see Fig. 11) and can be computed according to the laminated beam theory (see Appendix B), assuming that the beam is a laminate consisting of two laminae: sub-beam 1 is the first one, and sub-beam 2 is the second one. $V_1$ is the resultant of the shear stress in the cross section of the upper sub-beam. The total shear force is $V = \frac{F}{2}$. $V_1$ is determined by integrating the shear stress in the upper sub-beam, given by Eqs. (B.8) and (B.12):

$$V_1 = \int_{z_0}^{z_1} \tau_{zx}^1(z) w dz = Vw\left\{ -E_1\left[\frac{b}{2}(z_1^2 - z_0^2) + \frac{d}{6}(z_1^3 - z_0^3)\right] + c_1(z_1 - z_0)\right\} \tag{30}$$

where $z_0 = -\frac{h}{2}$ and $z_1 = z_0 + h_1$; $\tau_{zx}$ is the section shear stress, given by Eq. (B.8); $b$ is the bending–extension coupling compliance of the entire beam; $d$ is the bending compliance of the entire beam; and $c_1$ is integration constant, given by Eq. (B.10). Substituting the expression for the integration constant from Eq. (B.10) into (30) and performing analytical calculations, Eq. (30) becomes

$$V_1 = \frac{1}{12} V E_1 w h_1^2 [-6b + d(h_1 + 3h_2)] \tag{31}$$

We now employ Eqs. (B.2) and (B.4) to express the compliance coefficients $b$ and $d$ as functions of Young's moduli, $E_1$ and $E_2$, thicknesses, $h_1$ and $h_2$, and width, $w$. After analytical calculations, we get

$$V_1 = \frac{F}{2}\frac{E_1 h_1^2\left[E_1 h_1^2 + E_2\left(3h_2^2 + 4h_1 h_2\right)\right]}{E_1^2 h_1^4 + E_2^2 h_2^4 + 2E_1 E_2 h_1 h_2\left(2h_1^2 + 2h_2^2 + 3h_1 h_2\right)} \tag{32}$$

By setting the ratios $e = \frac{E_2}{E_1}$ and $r = \frac{h_2}{h_1}$, the expressions for the section shear force $V_1$ and bending component of the contact force, $Y_b$, can respectively take the form

$$V_1 = \frac{F}{2}\frac{1 + e(3r^2 + 4r)}{1 + e^2 r^4 + 2er(2 + 2r^2 + 3r)} \quad \text{and} \quad Y_b = \frac{F}{2}\frac{1}{1 + er^3} \tag{33}$$

#### 4.2.4. Specimen design criterion

Substituting Eqs. (33) into (29) and performing some analytical calculations, we obtain the following design criterion for the AENF specimen:

$$\frac{h_2}{h_1} = \sqrt{\frac{E_1}{E_2}} \tag{34}$$

We observe that this design criterion coincides with the respective criterion for the ADCB test configuration. In addition, Ouyang and Li [30] reached the same design criterion employing a different modeling approach, which strongly implies its correctness and

appropriateness compared to the counterpart criterion discussed in Section 2.2.

## 5. Numerical validation

The obtained specimen design criteria for the ADCB and AENF test configurations are validated here using two-dimensional FEAs.

### 5.1. Methods applied and input data

Two finite element models were created in Abaqus [42] for the ADCB and AENF test configurations, using four-node incompatible plane-stress elements (CPS4I), capable of correctly capturing bending. An element size of 0.1 mm was used to ensure a minimum of 10 elements through the thickness.

Three typical materials were employed: aluminum, steel, and AS4/8552. The latter is a unidirectional carbon/epoxy composite [43]. The elastic properties of these three materials are given in Table 1. Three bimaterial configurations were studied using the three materials: aluminum–AS4/8552, aluminum–steel, and AS4/8552 with a [90°//0°] layup, where the double slash denotes the position of the delamination plane.

In the models for both the ADCB and AENF test configurations, the specimen width, thickness, and initial crack length are $w = 15$ mm, $h = 5$ mm, and $a = 40$ mm. A span length $2L = 100$ mm was used in the AENF test. For each of the three bimaterial configurations, using the Young's moduli in Table 1 and the decoupling conditions given by Eq. (23) or (34), also considering that $h_1 + h_2 = h$, we determined the thicknesses of each sub-beam. Table 2 provides these thickness values.

All forces and displacement constraints introduced were nodal. In the AENF test, the interaction between the two cracked arms was implemented in the model to prevent interpenetration, without considering effects of friction. The applied force was $F = 30$ N for the ADCB configuration and $F = 500$ N for the AENF configuration.

The modal contributions to the ERR, $G_I$ and $G_{II}$, were obtained *locally* using the VCCT [44,45]. As this local method uses nodal forces and displacements at the crack tip associated to mode I and mode II, the contribution of each mode was obtained. The total ERR, $G$, was determined both by adding the two modal contributions to the ERR and in a global way (termed *global method* here), as the difference in coenergy due to a small crack advance, according to Eq. (A.11). In this global method, the displacement, $\Delta$, of the force-application point is determined for the same force, for two increments of the crack length, $a$ and $(a + \Delta a)$. Then, the total ERR is determined as

$$G = \frac{F}{2}(\Delta_{a+\Delta a} - \Delta_a) \tag{35}$$

where $\Delta$ is the relative displacement between the two force-application points in the ADCB test configuration and the displacement of the force-application point in the AENF test configuration.

### 5.2. Results for the ADCB test configuration

Table 3 provides the mode I and II contributions to the ERR obtained from the VCCT, the total ERR resulted by the algebraic sum of the two modal contributions, and the associated mode mixity, $G_{II}/G$. The table also presents the total ERR obtained from the global method. We observe that the introduced mode mixity is very small (less than 1.1%) in all bimaterial configurations studied, which implies that the specimen design criterion used is accurate enough in designing ADCB test specimens that experience (nearby) pure mode I conditions. Moreover, we observe that for all bimaterial configurations, the total ERR obtained *locally*, using the forces and displacements at the crack tip, agrees with that obtained *globally*, using the applied force and displacement of the force-application point; the difference is lower than 1.2% in all cases.

### 5.3. Results for the AENF test configuration

Table 4 presents the mode I and mode II contributions to the ERR obtained from the VCCT, the total ERR obtained as the sum of the two modal contributions, the associated mode mixity, $G_{II}/G$, and the total ERR obtained from the global method. We observe that the undesirable mode mixity, $G_I/G$, is very small (less than 2%) in all bimaterial configurations investigated, implying that the specimen design formula employed is accurate enough in designing AENF test specimens that experience (nearby) pure mode II conditions. Moreover, we observe that the relative difference between the VCCT and the global method in the calculation of the total ERR is satisfactorily low, lower than 1.9% in all bimaterial cases.

## 6. Conclusions and concluding remarks

This paper first reviewed existing proposals to achieve pure-mode fracture and then collected and discussed existing mode decoupling conditions for the ADCB test configuration. The literature basically uses two different specimen design criteria, so our review aimed to elucidate which one is ultimately correct. To support this, we proceeded to derive specimen design formulae to respectively obtain pure modes I and II in ADCB and AENF tests on bimaterial joints from scratch. To achieve this, we performed mechanical modeling of the ADCB and AENF specimens employing laminated beam theory, Engesser–Castigliano's theorem, unit-load

**Table 1**
Young's moduli, shear moduli, and Poisson's ratios of the materials employed.

| Material | $E_{ii}$ (GPa) | $G_{ij}$ (GPa) | $\nu_{ij}$ (-) |
|---|---|---|---|
| Aluminum | 70.0 | 26.9 | 0.300 |
| Steel | 210.0 | 80.8 | 0.300 |
| AS4/8552 | $E_{11}$: 135.0; $E_{22}$: 9.6 | $G_{12}$: 5.6; $G_{23}$: 3.4 | $\nu_{12}$: 0.320; $\nu_{23}$: 0.487 |

**Table 2**
Thicknesses of the bimaterial specimens studied.

| Bimaterial configuration [a] | $h_1$ (mm) | $h_2$ (mm) |
|---|---|---|
| Aluminum–AS4/8552 | 2.907 | 2.093 |
| Aluminum–steel | 3.171 | 1.829 |
| AS4/8552, [90°//0°] | 3.946 | 1.054 |

[a] In each bimaterial configuration, the first material corresponds to sub-beam 1 and the second one to sub-beam 2.

**Table 3**
Mode I, mode II, and total ERRs for the ADCB test configuration.

| Bimaterial configuration | VCCT | | | | Global method | Difference, VCCT–global (%) |
|---|---|---|---|---|---|---|
| | $G_I$ (N/m) | $G_{II}$ (N/m) | $G$ (N/m) | $G_{II}/G$ (%) | $G$ (N/m) | |
| Aluminum–AS4/8552 | 61.5 | 0.7 | 62.2 | 1.1% | 62.0 | 0.3% |
| Aluminum–steel | 50.1 | 1.0 | 51.1 | 2.0% | 50.5 | 1.2% |
| AS4/8552, [90°//0°] | 339.6 | 1.6 | 341.2 | 0.5% | 340.3 | 0.3% |

**Table 4**
Mode I, mode II, and total ERRs for the AENF configuration.

| Bimaterial configuration | VCCT | | | | Global method | Difference, VCCT–global (%) |
|---|---|---|---|---|---|---|
| | $G_I$ (N/m) | $G_{II}$ (N/m) | $G$ (N/m) | $G_{II}/G$ (%) | $G$ (N/m) | |
| Aluminum–AS4/8552 | 8.4 | 695.5 | 703.9 | 98.8% | 700.0 | 0.6% |
| Aluminum–steel | 11.8 | 579.4 | 591.2 | 98.0% | 580.0 | 1.9% |
| AS4/8552, [90°//0°] | 2.6 | 2,673.0 | 2,676.0 | 99.9% | 2,625.0 | 1.9% |

method, and equilibrium conditions. FEAs based on the VCCT were performed, and the numerical results validated the accuracy of the provided specimen design formulae.

We observed that the specimen design criteria for the ADCB (Eq. (23)) and AENF (Eq. (34)) test specimens are identical in the case that both sub-beams are homogeneous and special orthotropic. In other words, the same specimen design in terms of sub-beam thicknesses and Young's moduli can be used to characterize both mode I and mode II fractures. This finding is aligned with specimen design formulae reported in the literature (see Section 2). This agreement of the present work with part of the literature is a solid indication of which are the correct mode decoupling conditions and the associated specimen design formulae to be used in the future.

Bimaterial ADCB and AENF specimens that respect the reported design criteria can be tested using standard methodologies of testing in pure modes I and II to obtain the mode I and II fracture toughnesses, $G_{Ic}$ and $G_{IIc}$, respectively. Standard test procedures [46–49], based on the compliance calibration method, could be used for determining the pure-mode ERR values. In that case, the elastic properties of the two sub-beams are not necessary to be known, and only the crack length should be monitored during the test.

We close this section with a reference to well documented effects such as the elastic foundation effect in the ADCB specimen or the effect of crack-tip shear deformation [50–53]. These crack-tip effects are related to normal and shear stresses that appear near the crack tip in fracture tests, influencing the displacements and the ERR obtained in analytical approaches. However, the present analytical model does not consider such effects, as already mentioned; this simplification can be explained as follows. In the ADCB case, it was shown that the relative tangential displacement in the cracked region can be determined without considering crack-tip effects, whatever they are. In addition, in the AENF case, the decoupling condition dictates the absence of interfacial normal stresses in the uncracked region, so the uncracked region behaves as a monolithic beam. In other words, considering those effects was not necessary to obtain specimen design criteria for both the ADCB and AENF configurations.

## CRediT authorship contribution statement

**Faustino Mujika:** Conceptualization, Methodology, Validation, Formal analysis, Writing – original draft, Writing – review & editing, Project administration, Supervision, Funding acquisition. **Panayiotis Tsokanas:** Conceptualization, Methodology, Validation, Writing – original draft, Writing – review & editing, Visualization, Project administration. **Ainhoa Arrese:** Methodology, Software,

Formal analysis. **Paolo S. Valvo:** Conceptualization, Writing – original draft, Writing – review & editing. **Lucas F.M. da Silva:** Writing – review & editing, Supervision, Funding acquisition.

## Declaration of Competing Interest

The authors declare that they have no known competing financial interests or personal relationships that could have appeared to influence the work reported in this paper.

## Data availability

Data will be made available on request.

## Acknowledgements

F.M. and A.A. gratefully acknowledge the financial support of the University of the Basque Country (UPV/EHU) in the Research Group GIU20/060 "Mechanics of Materials". P.T. and L.F.M.d.S. gratefully acknowledge the financial support by the Foundation for Science and Technology (FCT) through the Project No. PTDC/EME-EME/6442/2020. Open Access funding was provided by the University of the Basque Country.

## A. Engesser–Castigliano's theorem and ERR

We assume an elastic body loaded by generalized concentrated forces, $F_j$. The generalized displacement of the application point of each force, $F_j$, in its direction, is $\delta_j$. In an infinitesimal crack advance, $da$, the work carried out in infinitesimal displacements, $d\delta_j$, is

$$dW = dU + Gwda \tag{A.1}$$

where $dW$ is the work done by the applied forces, $dU$ is the change in strain energy, $G$ is the energy needed for crack advance (per unit area), and $w$ is the width of the crack. The differential work done by the forces $F_j$ in their respective displacements $\delta_j$, assuming the repeated index convention, is

$$dW = F_j d\delta_j \tag{A.2}$$

Thus, Eq. (A.1) becomes

$$dU = F_j d\delta_j - Gwda \tag{A.3}$$

We assume that the strain energy is a thermodynamic state function depending on the displacements, $\delta_j$, and the crack length, $a$:

$$dU = \left(\frac{dU}{d\delta_j}\right)_a d\delta_j + \left(\frac{dU}{da}\right)_{\delta_j} da \tag{A.4}$$

Identifying terms in Eqs. (A.3) and (A.4), we have

$$F_j = \left(\frac{dU}{d\delta_j}\right)_a \tag{A.5}$$

and

$$G = -\frac{1}{w}\left(\frac{dU}{da}\right)_{\delta_j} \tag{A.6}$$

Eq. (A.5) is the first Castigliano's theorem, and Eq. (A.6) yields the ERR.

Next, the complementary strain energy, or coenergy, $C$, is defined as

$$C \equiv U^* = F_j\delta_j - U \tag{A.7}$$

The term *coenergy* is basically applied in the case of magnetic forces [54] but has also been used in mechanics [55]. In the present study, it is adopted for the complementary strain energy in the mechanical case. Differentiating Eq. (A.7) and substituting Eq. (A.3), we get

$$dC = \delta_j dF_j + Gwda \tag{A.8}$$

Assuming that the coenergy is a thermodynamic state function depending on the generalized forces, $F_j$, and the crack length, $a$, we have

$$dC = \left(\frac{dC}{dF_j}\right)_a dF_j + \left(\frac{dC}{da}\right)_{F_j} da \tag{A.9}$$

Identifying terms in Eqs. (A.8) and (A.9), we get

$$\delta_j = \left(\frac{dC}{dF_j}\right)_a \tag{A.10}$$

and

$$G = \frac{1}{w}\left(\frac{dC}{da}\right)_{F_j} \tag{A.11}$$

Eq. (A.10) is Engesser's first theorem or the generalized form of Castigliano's second theorem [8], so the denomination *Engesser–Castigliano's theorem* is used in this paper. Eq. (A.11) yields the ERR.

## B. Laminated beam theory

Basic elements of the first-order shear deformation theory (e.g., [56]) are presented here, necessary for determining the specimen design formula for the AENF configuration (Section 4.2.1).

We consider a beam with a rectangular cross section and thickness of $h$, made of $n$ orthotropic laminae of arbitrary thicknesses, as shown in Fig. B.1. The reference system, $Oyz$, is located in the mid-thickness plane of the beam, while the axial direction of the beam coincides with one of the principal directions of orthotropy of each lamina. The derivations below are based on the following main assumptions: (i) The axial strains are linearly distributed through the thickness of the beam; (ii) plane-stress state prevails in the $zx$-plane, and the out-of-plane stress is zero; (iii) all laminae are orthotropic and their stress–strain behavior is linear elastic; and (iv) residual thermal stresses are not considered.

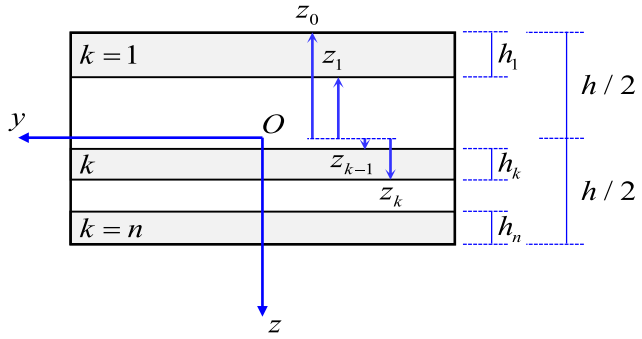


**Fig. B.1.** Cross section of a laminated beam consisting of $n$ laminae.

### B.1. Constitutive relations

The section force measures and strain measures are related as follows:

$$\begin{Bmatrix} N \\ M \end{Bmatrix} = \begin{bmatrix} A & B \\ B & D \end{bmatrix} \begin{Bmatrix} \varepsilon_0 \\ \kappa \end{Bmatrix} \tag{B.1}$$

where $N$ and $M$ are the section axial force and section bending moment, respectively; $\varepsilon_0$ and $\kappa$ are the axial strain and bending curvature of the middle plane, respectively; and $A$, $B$, and $D$ are the extensional stiffness coefficient, bending–extension coupling stiffness coefficient, and bending stiffness coefficient, respectively, given as

$$A = w\sum_{k=1}^{n} E_k(z_k - z_{k-1}), \qquad B = \frac{w}{2}\sum_{k=1}^{n} E_k\left(z_k^2 - z_{k-1}^2\right), \qquad \text{and} \qquad D = \frac{w}{3}\sum_{k=1}^{n} E_k\left(z_k^3 - z_{k-1}^3\right) \tag{B.2}$$

In Eqs. (B.2), $E_k$ is the longitudinal Young's modulus of the $k$-th lamina, while the ordinates $z_k$ and $z_{k-1}$ are schematically defined in Fig. B.1. The inverse form of Eq. (B.1) is

$$\begin{Bmatrix} \varepsilon_0 \\ \kappa \end{Bmatrix} = \begin{bmatrix} a & b \\ b & d \end{bmatrix} \begin{Bmatrix} N \\ M \end{Bmatrix} \tag{B.3}$$

where $a$, $b$, and $d$ respectively are the extensional compliance coefficient, bending–extension coupling compliance coefficient, and bending compliance coefficient, given as

$$a = \frac{D}{AD - B^2}, \qquad b = \frac{-B}{AD - B^2}, \qquad \text{and} \qquad d = \frac{A}{AD - B^2} \tag{B.4}$$

### B.2. Section axial and shear stresses

The axial stress in the $k$-th lamina is

$$\sigma_x^k = E_k(\varepsilon_0 + z\kappa) = E_k[N(a + bz) + M(b + dz)] \tag{B.5}$$

In each lamina, the following equilibrium equations must be satisfied:

$$\sigma_{x,x}^k + \tau_{zx,z}^k = 0 \quad \text{and} \quad \tau_{zx,x}^k + \sigma_{z,z}^k = 0 \tag{B.6}$$

Differentiating Eq. (B.5) and considering that $M_{,x} = V$, where $V$ is the section shear force, we get

$$\sigma_{x,x}^k = VE_k(b + dz) \tag{B.7}$$

Substituting Eq. (B.7) into the first equation of Eqs. (B.6) and integrating, the shear stress takes the form

$$\tau_{zx}^k(z) = V\left[-E_k\left(bz + d\frac{z^2}{2}\right) + c_k\right] \tag{B.8}$$

where $c_k$ are integration constants.

The boundary conditions for the shear stresses in each lamina are the following:

$$\tau_{zx}^1(z_0) = \tau_{zx}^n(z_n) = 0 \quad \text{and} \quad \tau_{zx}^{k-1}(z_{k-1}) = \tau_{zx}^k(z_{k-1}) \tag{B.9}$$

Substituting the first condition of Eqs. (B.9) into (B.8), $c_1$ is obtained as follows:

$$c_1 = E_1\left(bz_0 + d\frac{z_0^2}{2}\right) \tag{B.10}$$

Applying recursively the second boundary condition of Eqs. (B.9), $c_k$ are obtained as follows:

$$c_k = c_{k-1} + (E_k - E_{k-1})\left(bz_{k-1} + d\frac{z_{k-1}^2}{2}\right) \tag{B.11}$$

Eq. (B.11) can also be expressed as

$$c_k = E_1\left(bz_0 + d\frac{z_0^2}{2}\right) + \sum_{i=2}^{k}(E_i - E_{i-1})\left(bz_{i-1} + d\frac{z_{i-1}^2}{2}\right) \tag{B.12}$$

## References


[1] Tsokanas P, Fisicaro P, Loutas T, Valvo PS. Interfacial fracture toughness of unconventional specimens: some key issues. J Technol Exploit Mech Eng 2023;9(1):1–10. https://doi.org/10.35784/jteme.3361.

[2] Ouyang Z, Ji G, Li G. On approximately realizing and characterizing pure mode-I interface fracture between bonded dissimilar materials. J Appl Mech 2011;78(3):031020. https://doi.org/10.1115/1.4003366.

[3] Bennati S, Fisicaro P, Taglialegne L, Valvo PS. An elastic interface model for the delamination of bending-extension coupled laminates. Appl Sci 2019;9(17):3560. https://doi.org/10.3390/app9173560.

[4] Wang W, Lopes Fernandes R, Teixeira De Freitas S, Zarouchas D, Benedictus R. How pure mode I can be obtained in bi-material bonded DCB joints: a longitudinal strain-based criterion. Compos B Eng 2018;153:137–48. https://doi.org/10.1016/j.compositesb.2018.07.033.

[5] Boeman RG, Erdman DL, Klett LB, Lomax RD. A practical test method for mode I fracture toughness of adhesive joints with dissimilar substrates. SAMPE-ACCE-DOE Advanced Composites Conference, Detroit, MI. 1999.

[6] Mujika F, Insausti N, Isasa M, Boyano A. Geometric conditions for pure modes I and II in interlaminar fracture tests of bi-material specimens. In AP Vassilopoulos, V Michaud (Eds.), Proceedings of the 20th European Conference on Composite Materials, Vol. 4 (pp. 274–81). École Polytechnique Fédérale de Lausanne, Lausanne, Switzerland. 2022. http://doi.org/10.5075/epfl-298799_978-2-9701614-0-0.

[7] Rice JR. A path independent integral and the approximate analysis of strain concentration by notches and cracks. J Appl Mech 1968;35(2):379–86. https://doi.org/10.1115/1.3601206.

[8] Oden JT, Ripperger EA. Mechanics of elastic structures (2nd ed). McGraw-Hill; 1981.

[9] Williams JG. On the calculation of energy release rates for cracked laminates. Int J Fract 1988;36:101–19. https://doi.org/10.1007/BF00017790.

[10] Harvey CM. Mixed-mode partition theories for one-dimensional fracture. Doctoral dissertation, Loughborough University, 2012. https://hdl.handle.net/2134/10269.

[11] Schapery RA, Davidson BD. Prediction of energy release rate for mixed-mode delamination using classical plate theory. Appl Mech Rev 1990;43(5S):S281–7. https://doi.org/10.1115/1.3120829.

[12] Shahverdi M, Vassilopoulos AP, Keller T. Mixed-mode I/II fracture behavior of asymmetric adhesively-bonded pultruded composite joints. Eng Fract Mech 2014;115:43–59. https://doi.org/10.1016/j.engfracmech.2013.11.014.

[13] Shahverdi M, Vassilopoulos AP, Keller T. Mixed-mode I/II fracture behavior of asymmetric composite joints. Procedia Struct Integr 2016;2:1886–93. https://doi.org/10.1016/j.prostr.2016.06.237.
[14] Arouche MM, Wang W, Teixeira de Freitas S, de Barros S. Strain-based methodology for mixed-mode I+II fracture: a new partitioning method for bi-material adhesively bonded joints. J Adhes 2019;95(5–7):385–404. https://doi.org/10.1080/00218464.2019.1565756.
[15] Valvo PS. A revised virtual crack closure technique for physically consistent fracture mode partitioning. Int J Fract 2012;173:1–20. https://doi.org/10.1007/s10704-011-9658-y.
[16] Valvo PS. A further step towards a physically consistent virtual crack closure technique. Int J Fract 2015;192:235–44. https://doi.org/10.1007/s10704-015-0007-4.
[17] Valvo PS. A physically consistent virtual crack closure technique accounting for contact and interpenetration. Procedia Struct Integr 2020;28:2350–69. https://doi.org/10.1016/j.prostr.2020.11.083.
[18] Wang S, Guan L. On fracture mode partition theories. Comput Mater Sci 2012;52(1):240–5. https://doi.org/10.1016/j.commatsci.2011.03.021.
[19] Wang S, Harvey CM. Mixed mode partition theories for one dimensional fracture. Eng Fract Mech 2012;79:329–52. https://doi.org/10.1016/j.engfracmech.2011.11.013.
[20] Harvey CM, Wang S. Mixed-mode partition theories for one-dimensional delamination in laminated composite beams. Eng Fract Mech 2012;96:737–59. https://doi.org/10.1016/j.engfracmech.2012.10.001.
[21] Wang S, Harvey CM, Guan L. Partition of mixed modes in layered isotropic double cantilever beams with non-rigid cohesive interfaces. Eng Fract Mech 2013;111:1–25. https://doi.org/10.1016/j.engfracmech.2013.09.005.
[22] Valvo PS. On the calculation of energy release rate and mode mixity in delaminated laminated beams. Eng Fract Mech 2016;165:114–39. https://doi.org/10.1016/j.engfracmech.2016.08.010.
[23] Tsokanas P, Loutas T. Fracture mode partitioning: a review. (manuscript under review).
[24] Ouyang Z, Ji G, Li G, Pang S, Ibekwe S. A new idea of pure mode-I fracture test of bonded bi-materials. In: Proceedings of the ASME 2010 Pressure Vessels and Piping Conference, 3. Bellevue, Washington, USA: ASME; 2010. p. 53–60. https://doi.org/10.1115/PVP2010-25759.
[25] Zambelis G, Da Silva Botelho T, Klinkova O, Tawfiq I, Lanouette C. Evaluation of the energy release rate in mode I of asymmetrical bonded composite/metal assembly. Eng Fract Mech 2018;190:175–85. https://doi.org/10.1016/j.engfracmech.2017.12.007.
[26] Jiang Z, Wan S, Wu Z. Calculation of energy release rate for adhesive composite/metal joints under mode-I loading considering effect of the non-uniformity. Compos B Eng 2016;95:374–85. https://doi.org/10.1016/j.compositesb.2016.04.001.
[27] Khoshravan M, Asgari Mehrabadi F. Fracture analysis in adhesive composite material/aluminum joints under mode-I loading; experimental and numerical approaches. Int J Adh Adh 2012;39:8–14. https://doi.org/10.1016/j.ijadhadh.2012.06.005.
[28] Shimamoto K, Sekiguchi Y, Sato C. Effects of surface treatment on the critical energy release rates of welded joints between glass fiber reinforced polypropylene and a metal. Int J Adh Adh 2016;67:31–7. https://doi.org/10.1016/j.ijadhadh.2015.12.022.
[29] Shimamoto K, Sekiguchi Y, Sato C. The critical energy release rate of welded joints between fiber-reinforced thermoplastics and metals when thermal residual stress is considered. J Adhes 2016;92(4):306–18. https://doi.org/10.1080/00218464.2015.1031339.
[30] Ouyang Z, Li G. Nonlinear interface shear fracture of end notched flexure specimens. Int J Solids Struct 2009;46(13):2659–68. https://doi.org/10.1016/j.ijsolstr.2009.02.011.
[31] Liu Z, Huang Y, Yin Z, Bennati S, Valvo PS. A general solution for the two-dimensional stress analysis of balanced and unbalanced adhesively bonded joints. Int J Adh Adh 2014;54:112–23. https://doi.org/10.1016/j.ijadhadh.2014.05.011.
[32] Tsokanas P, Loutas T. Closed-form solution for interfacially cracked layered beams with bending-extension coupling and hygrothermal stresses. Eur J Mech A Solids 2022;96:104658. https://doi.org/10.1016/j.euromechsol.2022.104658.
[33] Garulli T, Catapano A, Fanteria D, Huang W, Jumel J, Martin E. Experimental assessment of fully-uncoupled multi-directional specimens for mode I delamination tests. Compos Sci Technol 2020;200:108421. https://doi.org/10.1016/j.compscitech.2020.108421.
[34] Garulli T, Catapano A, Fanteria D, Jumel J, Martin E. Design and finite element assessment of fully uncoupled multi-directional layups for delamination tests. J Compos Mater 2020;54(6):773–90. https://doi.org/10.1177/0021998319868293.
[35] Yokozeki T. Energy release rates of bi-material interface crack including residual thermal stresses: application of crack tip element method. Eng Fract Mech 2010;77(1):84–93. https://doi.org/10.1016/j.engfracmech.2009.09.018.
[36] Tsokanas P, Loutas T. Hygrothermal effect on the strain energy release rates and mode mixity of asymmetric delaminations in generally layered beams. Eng Fract Mech 2019;214:390–409. https://doi.org/10.1016/j.engfracmech.2019.03.006.
[37] Davidson P, Waas AM, Yerramalli CS. Experimental determination of validated, critical interfacial modes I and II energy release rates in a composite sandwich panel. Compos Struct 2012;94(2):477–83. https://doi.org/10.1016/j.compstruct.2011.08.007.
[38] Jespersen KM, Ota H, Harada K, Hosoi A, Kawada H. Experimental measurement of mode-I fracture toughness of dissimilar material joints with thermal residual stresses. Eng Fract Mech 2020;238:107249. https://doi.org/10.1016/j.engfracmech.2020.107249.
[39] Anderson TL. Fracture mechanics: fundamentals and applications (3rd ed). CRC Press; 2005. https://doi.org/10.1201/9781420058215.
[40] Arrese A, Boyano A, De Gracia J, Mujika F. A novel procedure to determine the cohesive law in DCB tests. Compos Sci Technol 2017;152:76–84. https://doi.org/10.1016/j.compscitech.2017.09.012.
[41] Sørensen BF, Kirkegaard P. Determination of mixed mode cohesive laws. Eng Fract Mech 2006;73(17):2642–61. https://doi.org/10.1016/j.engfracmech.2006.04.006.
[42] Abaqus 6.12 User's Manual, SIMULIA, 2012.
[43] Hexcel 8552 AS4 Unidirectional Prepreg, Qualification Material Property Data Report. NCAMP Test Report Number CAM-RP-2010-002 Rev A, 2011.
[44] Rybicki EF, Kanninen MF. A finite element calculation of stress intensity factors by a modified crack closure integral. Eng Fract Mech 1977;9(4):931–8. https://doi.org/10.1016/0013-7944(77)90013-3.
[45] Bonhomme J, Argüelles A, Castrillo MA, Viña J. Computational models for mode I composite fracture failure: the virtual crack closure technique versus the two-step extension method. Meccanica 2010;45:297–304. https://doi.org/10.1007/s11012-009-9248-5.
[46] ISO 15024:2023. Fibre-reinforced plastic composites – Determination of mode I interlaminar fracture toughness, GIC, for unidirectionally reinforced materials. International Organization for Standardization, 2023.
[47] ISO 25217:2009. Adhesives – Determination of the mode 1 adhesive fracture energy of structural adhesive joints using double cantilever beam and tapered double cantilever beam specimens. International Organization for Standardization, 2009.
[48] ASTM D5528–13. Standard test method for mode I interlaminar fracture toughness of unidirectional fiber-reinforced polymer matrix composites. ASTM International 2013. https://doi.org/10.1520/D5528-13.
[49] ASTM D7905/D7905M-14. Standard test method for determination of the mode II interlaminar fracture toughness of unidirectional fiber-reinforced polymer matrix composites. ASTM International 2014. https://doi.org/10.1520/D7905_D7905M-14.
[50] Kiss B, Szekrényes A. Fracture and mode mixity analysis of shear deformable composite beams. Arch Appl Mech 2019;89:2485–506. https://doi.org/10.1007/s00419-019-01591-4.
[51] Yoshihara H, Satoh A. Shear and crack tip deformation correction for the double cantilever beam and three-point end-notched flexure specimens for mode I and mode II fracture toughness measurement of wood. Eng Fract Mech 2009;76(3):335–46. https://doi.org/10.1016/j.engfracmech.2008.10.012.
[52] Szekrényes A. Improved analysis of unidirectional composite delamination specimens. Mech Mater 2007;39(10):953–74. https://doi.org/10.1016/j.mechmat.2007.04.002.
[53] Jumel J, Budzik MK, Shanahan MER. Beam on elastic foundation with anticlastic curvature: application to analysis of mode I fracture tests. Eng Fract Mech 2011;78(18):3253–69. https://doi.org/10.1016/j.engfracmech.2011.09.014.

[54] Mawardi OB. On the concept of coenergy. J Frank Inst 1957;264(4):313–32. https://doi.org/10.1016/0016-0032(57)90190-4.
[55] Seeler KA. System dynamics. An introduction for mechanical engineers. Springer; 2014. https://doi.org/10.1007/978-1-4614-9152-1.
[56] Reddy JN. Mechanics of laminated composite plates and shells: theory and analysis (2nd ed). CRC Press; 2003. https://doi.org/10.1201/b12409.